ARTICLES
https://doi.org/10.1038/s41561-020-0558-5
nature geoscience

Palaeoproterozoic oxygenated oceans following the Lomagundi–Jatuli Event

Kaarel Mänd[1,2]✉, Stefan V. Lalonde[3], Leslie J. Robbins[4], Marie Thoby[3], Kärt Paiste[2,5], Timmu Kreitsmann[2], Päärn Paiste[2], Christopher T. Reinhard[6,7], Alexandr E. Romashkin[8], Noah J. Planavsky[4,7], Kalle Kirsimäe[2], Aivo Lepland[2,5,9,10] and Kurt O. Konhauser[1]

The approximately 2,220–2,060 million years old Lomagundi–Jatuli Event was the longest positive carbon isotope excursion in Earth history and is traditionally interpreted to reflect an increased organic carbon burial and a transient rise in atmospheric O_2. However, it is widely held that O_2 levels collapsed for more than a billion years after this. Here we show that black shales postdating the Lomagundi–Jatuli Event from the approximately 2,000 million years old Zaonega Formation contain the highest redox-sensitive trace metal concentrations reported in sediments deposited before the Neoproterozoic (maximum concentrations of Mo = 1,009 μg g^{-1}, U = 238 μg g^{-1} and Re = 516 ng g^{-1}). This unit also contains the most positive Precambrian shale U isotope values measured to date (maximum $^{238}U/^{235}U$ ratio of 0.79‰), which provides novel evidence that there was a transition to modern-like biogeochemical cycling during the Palaeoproterozoic. Although these records do not preclude a return to anoxia during the Palaeoproterozoic, they uniquely suggest that the oceans remained well-oxygenated millions of years after the termination of the Lomagundi–Jatuli Event.

The Palaeoproterozoic era (2,500–1,600 million years ago (Ma)) witnessed the longest positive carbon isotope ($\delta^{13}C_{carb}$ ($\delta^{13}C = [(^{13}C/^{12}C)_{sample}/(^{13}C/^{12}C)_{standard}] - 1)$) excursion in Earth's history, recorded in marine carbonates deposited worldwide between ~2,220 and 2,060 Ma—the Lomagundi–Jatuli Event (LJE)[1,2]. Marine carbonates are generally characterized by $\delta^{13}C_{carb}$ values that vary between −5‰ and 5‰ for most of Earth's history, whereas peak LJE $\delta^{13}C_{carb}$ values reach 10–15‰ (ref. [1]). There is ongoing debate regarding the processes that led to the LJE. The standard and most commonly accepted interpretation invokes an increased burial of ^{13}C-depleted organic carbon (C_{org}), which led to the ^{13}C enrichment of the dissolved inorganic carbon pool and positive $\delta^{13}C_{carb}$ (refs. [1,3]). This acceleration in C_{org} burial may have been the result of an increase in oxidative weathering and nutrient delivery to the oceans[3]. Using a simple isotope mass balance, it was estimated that between 5 and 9×10^{20} mol C_{org} was buried over 100 Myr, which corresponds to the release of O_2 equivalents that represent 12–22 times the present O_2 atmospheric pool. An ensemble of evidence points to atmospheric O_2 accumulation during the LJE, including proxies that indicate growth of the marine sulfate reservoir[4–6], elevated concentrations of redox sensitive elements (RSEs)[7–10] and evidence for locally oxic conditions[3,11]. However, others argued that the 'standard' interpretation of the LJE is difficult to reconcile with our understanding of the C and O cycles[12,13], and that there is a notable paucity of C_{org}-rich deposits at this time[14], the most basic tracer of an enhanced organic carbon burial. Further, the carbon isotope dynamics during and after the positive excursion are currently debated, and there are multiple interpretations of the LJE positive $\delta^{13}C_{carb}$ values that do not invoke elevated rates of organic carbon burial and oxygen release[13,15]. Therefore, additional constraints on carbon and oxygen cycling are clearly needed to refine our view of this time interval.

The standard interpretation suggests that oxygen release due to C_{org} burial must have significantly slowed down in the aftermath of the LJE. To test this, we present new redox tracer data from two correlative sections (OnZaP and OPH sections (Methods)) of the upper Zaonega Formation (ZF), a post-LJE mudstone–dolostone succession. We provide some of the most straightforward evidence for Proterozoic surface oxygenation. In fact, current redox proxy records are most consistent with increasing oxygenation in the aftermath of the LJE, which forces a re-evaluation of our basic view of this turbulent interval of Earth's history.

Age and geochemical signatures of the ZF

According to the latest U–Pb age constraints on a tuff horizon within the lower ZF, the formation was deposited at ~1,980 Ma, ~80 Myr after the proposed termination of the LJE[16]. This age model is consistent with the $\delta^{13}C_{carb}$ stratigraphy. In the Onega Basin, $\delta^{13}C_{carb}$ values in the lowermost ZF and underlying Tulomozero Formation are characterized by typical LJE values of ≥8‰ (ref. [17]), with $\delta^{13}C_{carb}$ in the preserved carbonate strata returning to normal marine values of ~0‰ further upsection[18]. In the OPH core, the studied section occurs after several hundred metres of stratigraphy—including cumulatively ~210 m of mudstone-dominated sediments—where carbonates bear a normal marine (and therefore post-LJE) $\delta^{13}C_{carb}$ signal[18]. Assuming a reasonable range of deposition rates for the mudstones—for example, 1–100 m Myr^{-1} (ref. [19])—the studied section of the ZF was deposited millions of years after the termination of the LJE in the Onega Basin.

[1]Department of Earth & Atmospheric Sciences, University of Alberta, Edmonton, Alberta, Canada. [2]Department of Geology, University of Tartu, Tartu, Estonia. [3]CNRS-UMR6538 Laboratoire Géosciences Océan, European Institute for Marine Studies, Plouzané, France. [4]Department of Geology & Geophysics, Yale University, New Haven, CT, USA. [5]CAGE—Centre for Arctic Gas Hydrate, Environment and Climate, Department of Geosciences, UiT The Arctic University of Norway, Tromsø, Norway. [6]School of Earth and Atmospheric Sciences, Georgia Tech, Atlanta, GA, USA. [7]NASA Astrobiology Institute Alternative Earths Team, University of California, Riverside, CA, USA. [8]Institute of Geology, Karelian Science Centre, Petrozavodsk, Russia. [9]Geological Survey of Norway (NGU), Trondheim, Norway. [10]Department of Geology, Tallinn University of Technology, Tallinn, Estonia. ✉e-mail: kaarel.mand@ualberta.ca

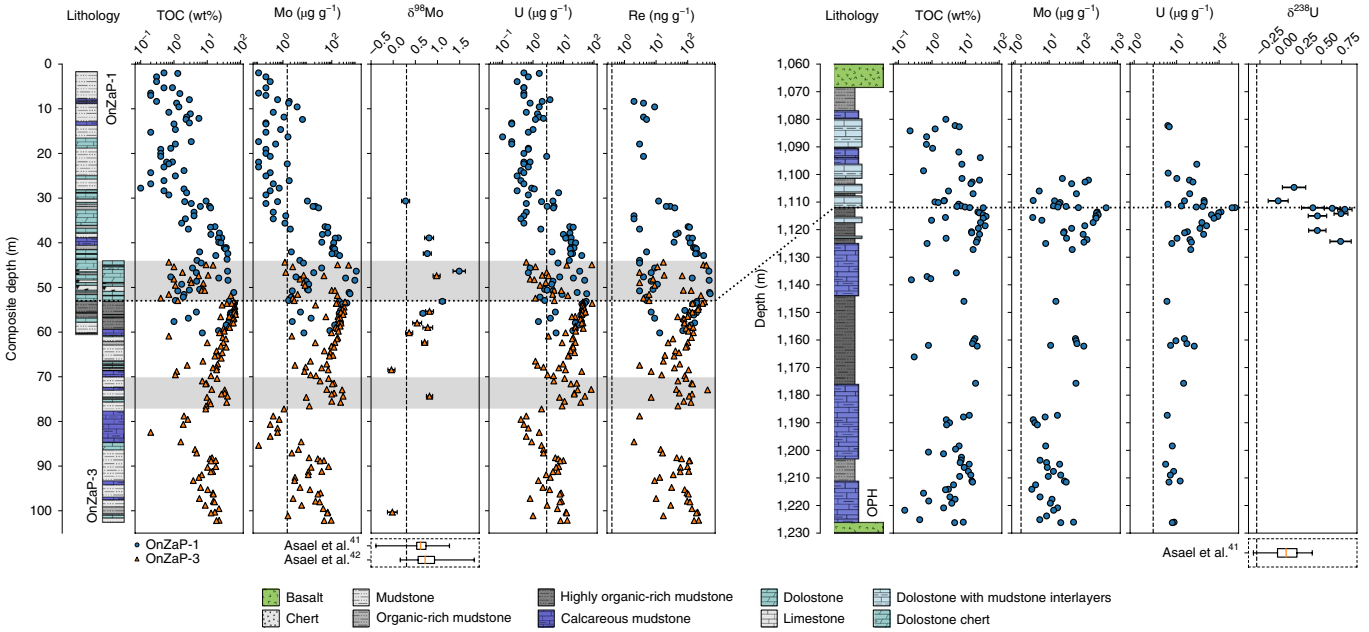

Fig. 1 | Lithology and geochemistry of the ZF. TOC and RSE profiles (errors contained within the symbols), and Mo and U isotope ratios ($\delta^{98}Mo$ ($\delta^{98}Mo = [(^{98}Mo/^{95}Mo)_{sample}/(^{98}Mo/^{95}Mo)_{standard}] - 1$) and $\delta^{238}U$ ($\delta^{238}U = [(^{238}U/^{235}U)_{sample}/(^{238}U/^{235}U)_{standard}] - 1$), error bars are 2 standard errors) are shown for the OnZaP (left) and OPH (right) sections. Vertical dashed lines are the average crustal values[30,31,48] and the dotted horizontal line is the phosphorus-rich mudstone–dolostone contact used for intrabasinal correlation (Methods and Supplementary Information). Box plots below the Mo and U isotope plots represent the distribution of previously published ZF data from lower in the succession (Supplementary Information)[41,42]. Grey horizontal bands show partly silicified and calcitized intervals due to fluid alteration[40]. Although these imply the presence of secondary fluids that could have mobilized RSE, microscale RSE distribution confirms the primary nature of the RSE enrichments (Supplementary Information).

The section is rich in total organic carbon (TOC), with average values of 27.4 ± 18.5 wt% in mudstones of the OnZaP section, and 14.5 ± 9.9 wt% in OPH mudstones (Fig. 1). These values are roughly comparable to the most organic-rich modern marine sediments (for example, up to 21.3 wt% on the Peru margin[20]). We focus specifically on Mo, U and Re enrichments, as these metals have provided robust evidence for major shifts in Earth's redox state[8,10,21]. In the Zaonega mudstones Mo, U and Re are significantly elevated relative to other Proterozoic black shales[8,10,21], with averages of 130 ± 142 μg g^{-1}, 19 ± 15 μg g^{-1} and 116 ± 84 ng g^{-1}, respectively, in OnZaP mudstones. In the OPH section, Mo and U average 71 ± 92 μg g^{-1} and 37 ± 50 μg g^{-1}, whereas the overall maximum Mo, U and Re concentrations across both sites are 1,009 μg g^{-1}, 238 μg g^{-1} and 516 ng g^{-1}, respectively. In the OnZaP section, $\delta^{98}Mo$ is on average 0.67 ± 0.81‰, with a maximum of 1.49 ± 0.14‰. U isotope values in the OnZaP section range from −0.03 to 0.79‰, with an average of 0.47‰. The maximum value is the most ^{238}U-enriched Precambrian shale measurement that has been reported to date[22,23].

The primary source of these RSE (in the rest of this article, RSE refers specifically to Mo, U and Re) to the oceans is the oxidative weathering of terrestrial RSE-bearing minerals (for example, pyrite and uraninite), and subsequent riverine transport as aqueous oxyanions[24,25]. Hydrothermal inputs, although not fully constrained at present, are not expected to be a quantitatively significant source for any of these RSEs[21,25]. The most important RSE sink is sequestration into marine sediments, which is influenced by the redox state of the depositional setting[24,26]. In oxic seawater, the RSEs are present as recalcitrant species that tend to accumulate in the water column[25,27], although Mo adsorbs to Mn(IV) oxides under oxic conditions and can then be released in pore waters after the reductive dissolution of Mn(IV) oxides in anoxic sediments[28]. In anoxic environments, the RSEs are progressively converted into particle-reactive species, which results in an efficient drawdown through authigenic sulfide precipitation or adsorption to organic matter[26,27]. With regards to Mo, it was found that the most efficient Mo sequestration takes place under euxinic waters with >11 μM sulfide (HS^-) (ref. [29]). In a broad sense, the contrasting behaviour of these elements in oxic and anoxic conditions ensures that the drawdown and marine reservoir sizes are governed by global ocean redox—large RSE reservoirs develop in an oxic ocean, which leads to large local sedimentary RSE enrichments under anoxic conditions[10,21].

The U and Mo isotope systems, similar to RSE enrichments, respond to the global marine redox landscape. There is consensus that well-oxygenated oceans are characterized by high Mo and U isotope values[30,31]. It is, however, difficult to gauge when a sedimentary archive captures seawater U and Mo isotope values. For instance, seawater Mo isotope values are most likely to be captured in shales deposited in isolated basins with high HS^- levels[32]. However, the non-quantitative reduction of Mo in euxinic marine basins results in negative fractionation and shale $\delta^{98}Mo$ values that are lower than those of seawater[30], and therefore $\delta^{98}Mo$ in euxinic shales is often interpreted as a minimum estimate for seawater $\delta^{98}Mo$ (ref. [11]). U isotope values in shales will be closest to the seawater values in oxic sediments and up to ~1‰ heavier than those of seawater in anoxic and high-productivity settings[31] (see Supplementary Information for a detailed discussion on Mo and U isotope values). Using this framework, our data points to well-oxygenated oceans with high rates of primary productivity during deposition of the ZF.

Marine RSE inventory

RSE enrichments in the ZF far exceed anything known from pre-Neoproterozoic black shales (Fig. 2). Similar values are found only in the Phanerozoic, where they have been taken as evidence for an expanded seawater RSE inventory, the direct result of pervasive ocean–atmosphere oxygenation[8,10,21]. We believe that the ZF, likewise, contains evidence of a large marine RSE inventory that

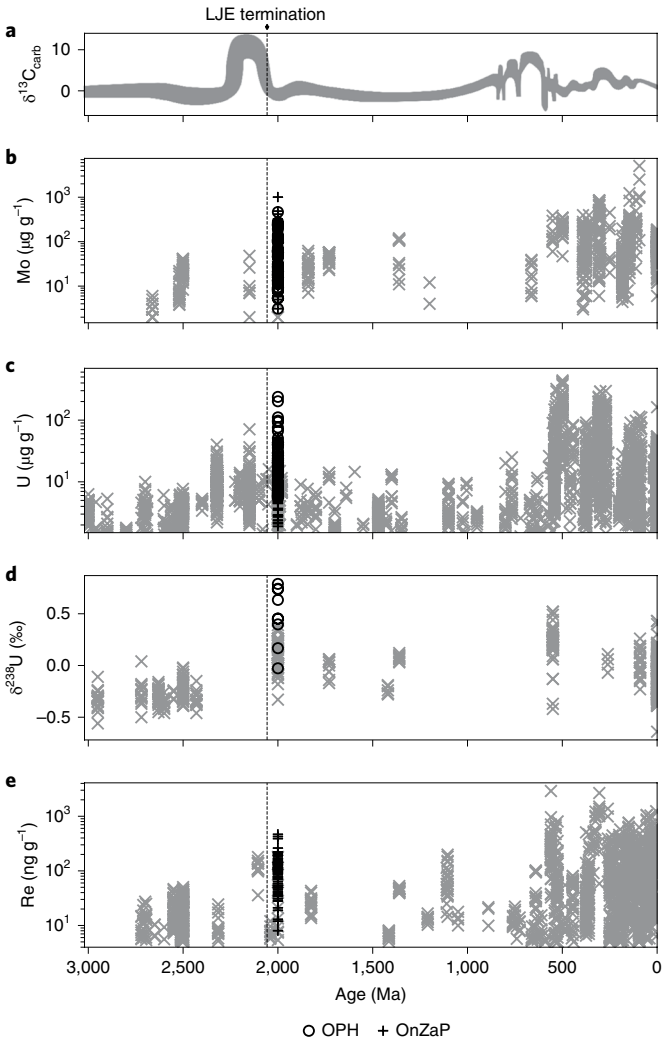

Fig. 2 | Secular trends in RSE concentrations from anoxic shales. ZF data (plus and circle symbols) are plotted on compilations from the literature (× symbols). **a**, Changes in $\delta^{13}C_{carb}$ through time, modified from Karhu[49]. **b**, Mo concentrations from Robbins et al.[50]. **c**, U concentrations from Partin et al.[8]. **d**, U isotope ratios from Wang et al.[22] and Yang et al.[23]. **e**, Re concentrations from Sheen et al.[10]. Concentration errors are within symbols; for $\delta^{238}U$ and age errors, refer to Fig. 1, Supplementary Information and the compilation data sources.

strongly suggests a relatively oxidized ocean–atmosphere system with a robust terrestrial oxic RSE weathering flux, in which the drawdown of RSE was limited by the relative scarcity of anoxic conditions on the seafloor. Further, U and Re enrichments—which, unlike Mo, are also drawn down in ferruginous waters[33]—suggest that this was an episode of thorough water column oxygenation on continental shelves, rather than just a restriction of euxinic deposition, >1,400 Myr before the terminal oceanic oxygenation during the Neoproterozoic[34].

Although low Mo in black shales could be explained by a small marine Mo pool, basinal restriction leading to localized Mo depletion[28] or inefficient Mo scavenging under low HS^- conditions[29], there are limited ways to explain the elevated RSE concentrations in black shales of the ZF (that is, up to several hundreds μg g^{-1} of Mo throughout the >160-km-wide basin). One possibility is anomalously low sedimentation rates, which have previously been invoked to explain the high TOC in U-rich black shales of the Miocene Monterey Formation, USA[35]. Although low sedimentation rates may have played a role in concentrating TOC and RSE in the ZF, the magnitude of the RSE enrichment—consistent with Phanerozoic levels (Fig. 2)—makes it unlikely that sedimentation rate alone could account for it. A more plausible explanation is that the ZF was also a highly efficient RSE sink that had reliable access to a large oceanic RSE inventory[28] (see Supplementary Information for additional discussion on factors that control the RSE accumulation).

The U isotope values provide an independent confirmation of highly oxygenated oceans—as noted above they are the most positive Precambrian shale $\delta^{238}U$ values measured to date (Fig. 2), which requires both high seawater $\delta^{238}U$ values (probably comparable to the modern value of about −0.4‰) and a near full expression of the equilibrium ~1.2‰ fractionation during U reduction. High seawater values only develop when oxic U burial is a major U burial flux in well-oxygenated oceans[36]. In addition, a significant positive U isotope fractionation (≫0.6‰) strongly suggests U reduction in the water column instead of within the sediment pile[31]. U reduction rates appear to scale with sulfate (or iron) reduction rates[37], which provides a link between amounts of organic matter loading in a marine system and the isotope fractionation that occurs during U burial. For reference, there is limited water column sulfate reduction in the modern Black Sea and Cariaco Basin because of low rates of productivity and the maximum sediment $\delta^{238}U$ is only ~0.8‰ and ~0.6‰ higher than seawater, respectively[36]. In contrast, a high productivity in the ZF is consistent with the anomalous C_{org} enrichments. Therefore, the strongly positive U isotope values in the ZF, along with the RSE enrichments, are most readily explained by invoking both globally well-oxygenated oceans and markedly elevated rates of local primary productivity, the latter of which would tend to enhance the expression of isotope effects associated with U reduction.

Conflicting views on oxygenation during ZF deposition

Our interpretation that the ZF records well-oxygenated ocean conditions is ostensibly in conflict with previous interpretations derived from C, S and Mo isotope records proposed to reflect global deoxygenation. However, much of this data can plausibly be explained through local rather than global processes. First, Kump et al.[38] postulated a post-LJE global negative $\delta^{13}C$ excursion based on depleted $\delta^{13}C$ in ZF carbonates and organic matter. This was interpreted to result from the widespread oxidation of organic-rich shales, which would have favoured suppressed, rather than elevated, O_2 levels. However, negative $\delta^{13}C$ in the ZF has subsequently been reinterpreted to reflect basin-wide methanotrophy and secondary overprinting of carbonate rocks[39]. Second, Scott et al.[5] argued that highly ^{34}S-enriched pyrites in the upper ZF reflect a global collapse of the marine sulfate reservoir due to deoxygenation. In contrast, Paiste et al.[40] explained the same trends through basin-specific processes that involve quantitative uptake of sulfate. Third, Asael et al.[41,42] inferred an ~0.7‰ seawater $\delta^{98}Mo$ value from two other cores in the upper ZF, identical to the average in the OnZaP section. Mn oxides, which form in oxic waters, preferentially scavenge ^{95}Mo and drive seawater $\delta^{98}Mo$ to higher values. If one assumes a modern riverine input value of ~0.7‰ for the Palaeoproterozoic[30], a seawater value of ~0.7‰ suggests limited Mn oxide precipitation and, thus, little O_2 in the oceans. However, the sequestration of Mo in sediments commonly imparts a negative $\delta^{98}Mo$ fractionation, except in highly restricted euxinic basins in which nearly all Mo is drawn down[30]. This highlights that the highest Mo isotope values of ~1.4‰ represent a minimum seawater $\delta^{98}Mo$ estimate (Canfield et al.[11] and Supplementary Information) and that the Mo isotope data does not necessarily preclude widespread oxic conditions.

Implications of oxygenated oceans at approximately 2,000 Ma

RSE-replete conditions during the deposition of the ZF have important implications for Earth's global C and O cycles during the

Palaeoproterozoic. Tracking the evolution of Earth's redox history is also critical to understand early eukaryote evolution. The late rise to prevalence of eukaryotes in the Neoproterozoic is thought to be linked to widespread anoxic and nutrient-poor conditions that favoured prokaryotic metabolisms[43]. Given the extent of ocean oxygenation and nutrient abundance inferred from the ZF[3,44], conditions favourable to eukaryotic diversification could have been present for much of the middle Palaeoproterozoic. It is curious, then, that molecular clock analyses and microfossil evidence of eukaryote origin tend to converge after ~1,900 Ma (refs. [45,46]). In the simplest sense, this discrepancy supports the central importance of a unique endosymbiosis event for the emergence of eukaryotes, rather than the removal or lessening of an environmental barrier.

The ZF is part of a well-recognized overall trend towards elevated RSE concentrations at ~2,400–2,000 Ma that has been linked to well-oxygenated oceanic–atmospheric conditions[8–10]. Surprisingly, our ZF data extend this trend past the termination of the LJE. Furthermore, the extreme RSE enrichments hint that, instead of being in decline, atmospheric O_2 abundance could still have been high perhaps several tens of million years after the canonical end of the LJE[16]. In the modern, well-oxygenated world, the geological O_2 response time is on the order of ~2 Myr (ref. [47]), whereas the residence times of Mo, U and Re in the oceans are ~440, ~400 and ~780 kyr, respectively[25,27]. Therefore, if the LJE decline is linked to a decrease in O_2 production as the result of diminishing C_{org} burial by the end of the LJE, then O_2 would be expected to be significantly attenuated by this time. Instead, our data suggest the opposite.

Our observations provide empirical evidence for models (for example, Miyazaki et al.[13]) that decouple the strongly positive carbonate carbon isotope values of the LJE from enhanced C_{org} burial. Further, given the likelihood that highly oxidized conditions continued up to ~2,000 Ma, this highlights the importance of exploring alternative interpretations of the carbon isotope record and the need for refined chemostratigraphic and geochronological studies focused on this key interval of Earth's history.

Online content

Any methods, additional references, Nature Research reporting summaries, source data, extended data, supplementary information, acknowledgements, peer review information; details of author contributions and competing interests; and statements of data and code availability are available at https://doi.org/10.1038/s41561-020-0558-5.

Received: 25 January 2019; Accepted: 19 February 2020;
Published online: 16 March 2020

References

1. Karhu, J. A. & Holland, H. D. Carbon isotopes and the rise of atmospheric oxygen. *Geology* **24**, 867–870 (1996).
2. Martin, A. P., Condon, D. J., Prave, A. R. & Lepland, A. A review of temporal constraints for the Palaeoproterozoic large, positive carbonate carbon isotope excursion (the Lomagundi-Jatuli Event). *Earth-Sci. Rev.* **127**, 242–261 (2013).
3. Bekker, A. & Holland, H. D. Oxygen overshoot and recovery during the early Paleoproterozoic. *Earth Planet. Sci. Lett.* **317–318**, 295–304 (2012).
4. Planavsky, N. J., Bekker, A., Hofmann, A., Owens, J. D. & Lyons, T. W. Sulfur record of rising and falling marine oxygen and sulfate levels during the Lomagundi event. *Proc. Natl Acad. Sci. USA* **109**, 18300–18305 (2012).
5. Scott, C. et al. Pyrite multiple-sulfur isotope evidence for rapid expansion and contraction of the early Paleoproterozoic seawater sulfate reservoir. *Earth Planet. Sci. Lett.* **389**, 95–104 (2014).
6. Blättler, C. L. et al. Two-billion-year-old evaporites capture Earth's great oxidation. *Science* **360**, 320–323 (2018).
7. Konhauser, K. O. et al. Aerobic bacterial pyrite oxidation and acid rock drainage during the Great Oxidation Event. *Nature* **478**, 369–373 (2011).
8. Partin, C. A. et al. Large-scale fluctuations in Precambrian atmospheric and oceanic oxygen levels from the record of U in shales. *Earth Planet. Sci. Lett.* **369–370**, 284–293 (2013).
9. Kipp, M. A., Stüeken, E. E., Bekker, A. & Buick, R. Selenium isotopes record extensive marine suboxia during the Great Oxidation Event. *Proc. Natl Acad. Sci. USA* **114**, 875–880 (2017).
10. Sheen, A. I. et al. A model for the oceanic mass balance of rhenium and implications for the extent of Proterozoic ocean anoxia. *Geochim. Cosmochim. Acta* **227**, 75–95 (2018).
11. Canfield, D. E. et al. Oxygen dynamics in the aftermath of the Great Oxidation of Earth's atmosphere. *Proc. Natl Acad. Sci. USA* **110**, 16736–16741 (2013).
12. Bachan, A. & Kump, L. R. The rise of oxygen and siderite oxidation during the Lomagundi Event. *Proc. Natl Acad. Sci. USA* **112**, 6562–6567 (2015).
13. Miyazaki, Y., Planavsky, N., Bolton, E. W. & Reinhard, C. T. Making sense of massive carbon isotope excursions with an inverse carbon cycle model. *J. Geophys. Res. Biogeosci.* **123**, 2485–2496 (2018).
14. Melezhik, V. A., Fallick, A. E., Medvedev, P. V. & Makarikhin, V. V. Extreme $^{13}C_{carb}$ enrichment in ca. 2.0 Ga magnesite-stromatolite-dolomite-'red beds' association in a global context: a case for the world-wide signal enhanced by a local environment. *Earth-Sci. Rev.* **48**, 71–120 (1999).
15. Eguchi, J., Seales, J. & Dasgupta, R. Great Oxidation and Lomagundi events linked by deep cycling and enhanced degassing of carbon. *Nat. Geosci.* **13**, 71–76 (2020).
16. Martin, A. P. et al. Multiple Palaeoproterozoic carbon burial episodes and excursions. *Earth Planet. Sci. Lett.* **424**, 226–236 (2015).
17. Melezhik, V. A., Fallick, A. E., Brasier, A. T. & Lepland, A. Carbonate deposition in the Palaeoproterozoic Onega basin from Fennoscandia: a spotlight on the transition from the Lomagundi–Jatuli to Shunga events. *Earth Sci. Rev.* **147**, 65–98 (2015).
18. Kreitsmann, T. et al. Hydrothermal dedolomitisation of carbonate rocks of the Paleoproterozoic Zaonega Formation, NW Russia—implications for the preservation of primary C isotope signals. *Chem. Geol.* **512**, 43–57 (2019).
19. Sadler, P. M. The influence of hiatuses on sediment accumulation rates. *GeoRes. Forum* **5**, 15–40 (1999).
20. Böning, P. et al. Geochemistry of Peruvian near-surface sediments. *Geochim. Cosmochim. Acta* **68**, 4429–4451 (2004).
21. Reinhard, C. T. et al. Proterozoic ocean redox and biogeochemical stasis. *Proc. Natl Acad. Sci. USA* **110**, 5357–5362 (2013).
22. Wang, X. et al. A Mesoarchean shift in uranium isotope systematics. *Geochim. Cosmochim. Acta* **238**, 438–452 (2018).
23. Yang, S., Kendall, B., Lu, X., Zhang, F. & Zheng, W. Uranium isotope compositions of mid-Proterozoic black shales: evidence for an episode of increased ocean oxygenation at 1.36 Ga and evaluation of the effect of post-depositional hydrothermal fluid flow. *Precambrian Res.* **298**, 187–201 (2017).
24. Dunk, R. M., Mills, R. A. & Jenkins, W. J. A reevaluation of the oceanic uranium budget for the Holocene. *Chem. Geol.* **190**, 45–67 (2002).
25. Miller, C. A., Peucker-Ehrenbrink, B., Walker, B. D. & Marcantonio, F. Re-assessing the surface cycling of molybdenum and rhenium. *Geochim. Cosmochim. Acta* **75**, 7146–7179 (2011).
26. Crusius, J., Calvert, S., Pedersen, T. & Sage, D. Rhenium and molybdenum enrichments in sediments as indicators of oxic, suboxic and sulfidic conditions of deposition. *Earth Planet. Sci. Lett.* **145**, 65–78 (1996).
27. Anderson, R. F., Fleisher, M. Q. & LeHuray, A. P. Concentration, oxidation state, and particulate flux of uranium in the Black Sea. *Geochim. Cosmochim. Acta* **53**, 2215–2224 (1989).
28. Algeo, T. J. & Lyons, T. W. Mo–total organic carbon covariation in modern anoxic marine environments: implications for analysis of paleoredox and paleohydrographic conditions. *Paleoceanography* **21**, PA1016 (2006).
29. Helz, G. R. et al. Mechanism of molybdenum removal from the sea and its concentration in black shales: EXAFS evidence. *Geochim. Cosmochim. Acta* **60**, 3631–3642 (1996).
30. Kendall, B., Dahl, T. W. & Anbar, A. D. The stable isotope geochemistry of molybdenum. *Rev. Mineral. Geochem.* **82**, 683–732 (2017).
31. Andersen, M. B., Stirling, C. H. & Weyer, S. Uranium isotope fractionation. *Rev. Mineral. Geochem.* **82**, 799–850 (2017).
32. Dickson, A. J. A molybdenum-isotope perspective on Phanerozoic deoxygenation events. *Nat. Geosci.* **10**, 721–726 (2017).
33. Tribovillard, N., Algeo, T. J., Lyons, T. & Riboulleau, A. Trace metals as paleoredox and paleoproductivity proxies: an update. *Chem. Geol.* **232**, 12–32 (2006).
34. Och, L. M. & Shields-Zhou, G. A. The Neoproterozoic oxygenation event: environmental perturbations and biogeochemical cycling. *Earth-Sci. Rev.* **110**, 26–57 (2012).
35. Föllmi, K. B. et al. Phosphogenesis and organic-carbon preservation in the Miocene Monterey Formation at Naples Beach, California—the Monterey hypothesis revisited. *Bull. Geol. Soc. Am.* **117**, 589–619 (2005).
36. Andersen, M. B. et al. A modern framework for the interpretation of $^{238}U/^{235}U$ in studies of ancient ocean redox. *Earth Planet. Sci. Lett.* **400**, 184–194 (2014).
37. Barnes, C. E. & Cochran, J. K. Uranium geochemistry in estuarine sediments: controls on removal and release processes. *Geochim. Cosmochim. Acta* **57**, 555–569 (1993).

38. Kump, L. R. et al. Isotopic evidence for massive oxidation of organic matter following the Great Oxidation Event. *Science* **334**, 1694–1696 (2011).
39. Qu, Y., Črne, A. E., Lepland, A. & van Zuilen, M. A. Methanotrophy in a Paleoproterozoic oil field ecosystem, Zaonega Formation, Karelia, Russia. *Geobiology* **10**, 467–478 (2012).
40. Paiste, K. et al. Multiple sulphur isotope records tracking basinal and global processes in the 1.98 Ga Zaonega Formation, NW Russia. *Chem. Geol.* **499**, 151–164 (2018).
41. Asael, D. et al. Coupled molybdenum, iron and uranium stable isotopes as oceanic paleoredox proxies during the Paleoproterozoic Shunga Event. *Chem. Geol.* **362**, 193–210 (2013).
42. Asael, D., Rouxel, O., Poulton, S. W., Lyons, T. W. & Bekker, A. Molybdenum record from black shales indicates oscillating atmospheric oxygen levels in the early Paleoproterozoic. *Am. J. Sci.* **318**, 275–299 (2018).
43. Brocks, J. J. et al. The rise of algae in Cryogenian oceans and the emergence of animals. *Nature* **548**, 578–581 (2017).
44. Lepland, A. et al. Potential influence of sulphur bacteria on Palaeoproterozoic phosphogenesis. *Nat. Geosci.* **7**, 20–24 (2014).
45. Parfrey, L. W., Lahr, D. J. G., Knoll, A. H. & Katz, L. A. Estimating the timing of early eukaryotic diversification with multigene molecular clocks. *Proc. Natl Acad. Sci. USA* **108**, 13624–13629 (2011).
46. Betts, H. C. et al. Integrated genomic and fossil evidence illuminates life's early evolution and eukaryote origin. *Nat. Ecol. Evol.* **2**, 1556 (2018).
47. Kasting, J. F. & Canfield, D. E. in *Fundamentals of Geobiology* (eds Knoll, A. H., Canfield, D. E. & Konhauser, K. O.) 93–104 (John Wiley & Sons, 2012).
48. McLennan, S. M. Relationships between the trace element composition of sedimentary rocks and upper continental crust: trace element composition and upper continental crust. *Geochem. Geophys. Geosyst.* **2**, 1021 (2001).
49. Karhu, J. A. in *Encyclopedia of Geochemistry* (eds Marshall, C. P. & Fairbridge, R. W.) 67–73 (Kluwer Academic Publishers, 1999).
50. Robbins, L. J. et al. Trace elements at the intersection of marine biological and geochemical evolution. *Earth-Sci. Rev.* **163**, 323–348 (2016).

Methods

Materials. The material for this study comes from drill cores in the Onega Basin that intersect the ZF—a relatively well-preserved 1,500 m-thick succession of organic-rich mudstones and carbonates, interlayered and intersected with igneous units, which include lavas, tuffs and sills (see Supplementary Information for a detailed geological setting)[51]. The 60-m-long cores OnZaP-1 and OnZaP-3 were drilled 500 m apart in the northeastern part of the Onega Basin near Shunga village, close to drill core FAR-DEEP 13A[40]. The OnZaP-1 and OnZaP-3 cores partly overlap and combined provide a 102-m-thick OnZaP section. The 3,500-m-long OPH core that intersects the entire supracrustal succession of the Onega Basin was drilled ~60 km to the south. Paiste et al.[40,52] correlated the upper ZF OnZaP and OPH sections based on C isotopes, trace metal enrichments, P concentrations and a distinct massive P-rich dolomite unit that occurs throughout the Onega Basin.

The lithology of this section is characterized by alternating dolomite- to calcite-rich carbonates and exceptionally organic-rich mudstones that are intersected by silica or pyrobitumen veins (Fig. 1). In the OnZaP section, the interval from the bottom of the section to 53 m depth is dominated by highly organic-rich mudstones with relatively few carbonate beds, the 53–33 m interval is mostly dolostone and contains a distinctive dolomite unit and the 33–1.7 m interval consists of grey mudstones and marly carbonate beds[40]. Two sets of samples from the OnZaP section were analysed in this study. Set MSP0001 consists of 135 samples that were taken at roughly 1 m intervals and is identical to that used in Paiste et al.[40]. Set MSP0010 contains 79 samples that more specifically targeted RSE and organic-rich intervals. A set of 89 samples was analysed from the 1,060–1,230 m interval of the OPH core that is roughly equivalent to the OnZaP section.

Elemental concentrations. The TOC contents of the MSP0001 and OPH samples were adapted from Paiste et al.[40] and were measured from powdered aliquots using a LECO SC-444 analyser at the Geological Survey of Norway. The detection limit was 0.1 wt% and the precision better than 10%. For the MSP0010 set, TOC was measured at the Pôle Spectrométrie Océan, European Institute for Marine Studies. Dried and powdered samples were combusted in ceramic beakers at 500 °C for 24 h and the loss of mass on ignition was determined. Repeat measurements of seven samples generally differed by <1 wt%.

Major and trace element compositions of the MSP0001 samples were determined at Acme Labs. The samples were first pulverized and combusted to remove organic carbon. For major elements, the sample was fused in $LiBO_2$ flux and then digested, whereas minor elements were analysed from full digests in HNO_3, $HClO_4$ and HF. Measurements utilized inductively coupled plasma optical emission spectrometry or inductively coupled plasma mass spectrometry (ICP-MS). Average relative standard deviation was less than 5% for all the elements. The MSP0010 element composition was determined at the European Institute for Marine Studies. Samples were pulverized in a tungsten carbide crusher and an agate mill, then combusted at 500 °C for 24 h to remove C_{org}. Major element concentrations were measured on a Jobin Yvon Horiba Ultima 2 inductively coupled plasma optical emission spectrometer after digestion overnight at 80 °C in concentrated HF and HNO_3 and neutralization with boric acid to retain Si. For trace element concentrations, digestion was performed in a class 1000 clean laboratory using distilled acids—samples mixed with concentrated HF and HNO_3 were heated to 80 °C overnight, then allowed to evaporate; this digestion was then repeated with concentrated aqua regia, after which the sample was taken up in 6 M HCl. Trace element concentrations were measured on a Thermo Scientific Element 2 ICP-MS calibrated against commercial multi-element standards and digested geostandards (for example, BHVO-2). OPH major and trace elements were measured on a Philips PW 1480 X-ray fluorescence spectrometer equipped with a Rh X-ray tube at the Geological Survey of Norway. For the major elements, 0.6 g of a ground and combusted (1,000 °C) sample was fused into a bead in a CLAISSE FLUXER-BIS together with 4.2 g of $Li_2B_4O_7$. For the trace elements, 2.4 g of Hoechst wax was mixed with 9.6 g of sample in a Spex Mixer/Mill and pressed into a pellet using a Herzog pelletizing press. Major element detection limits were 0.01% (P_2O_5, CaO), 0.5% (SiO_2), 0.02% (Al_2O_3) and 0.02% (MgO), and the precision (1σ) was typically ~2%. Detection limits for trace elements were $\leq 10\,\mu g\,g^{-1}$.

Samples with a ratio of $(CaO + MgO)/(SiO_2 + Al_2O_3) > 0.2$—approximating >20 wt% carbonate content—were excluded when calculating Mo, U and Re averages, as compilations of RSE in black shales generally only include shale samples[8,10,21]. An exception was made for samples with >5 wt% TOC, since such sediments would have played a role in trace metal cycling regardless of their mineralogical composition.

Mo isotopes. Mo isotopes were measured from fully digested OnZaP MSP0010 samples that were purified via column chromatography according to Ref. [41]. A ^{97}Mo–^{100}Mo double spike was employed[53] and the isotopes were measured on a Thermo Scientific Neptune multi-collector ICP-MS at IFREMER, Brest, France. Data is expressed relative to NIST SRM 3134 = 0.25‰[54]. Detailed methodology is provided in the Supplementary Information.

U Isotopes. Samples for U isotopes were sequentially digested in a mixture of 3 ml of HNO_3 and 1 ml of HF at 100 °C for 24 h, then aqua regia at 95 °C for 24 h. After each digestion step, the sample was evaporated to dryness. Sample residues were taken up in 5 ml of 3 M HNO_3 at 70 °C. All the sample preparation was performed in a Pico-trace clean lab at the Yale Metal Geochemistry Center. U isotope values were measured on a Thermo Neptune Multi-collector ICP-MS following the method in Wang et al.[22] using the IRMM-3636 233/236 U double spike. Accuracy and precision were monitored with concentration-matched CRM112, CRM129a and Ricca geostandards. Error was less than 0.15‰. A detailed methodology is provided in the Supplementary Information.

Data availability

The novel ZF geochemical data presented here will be available in the PANGAEA data repository at https://doi.org/10.1594/PANGAEA.911670 (drill cores OnZaP-1 and 3[55]) and https://doi.org/10.1594/PANGAEA.911674 (drill core OPH[56]). Geochemical Source Data and raw images for Supplementary Figures are available at figshare (https://doi.org/10.6084/m9.figshare.11674056/). Source Data for Figs. 1 and 2 are available as Source Data files.

References

51. Melezhik, V. A., Fallick, A. E., Filippov, M. M. & Larsen, O. Karelian shungite—an indication of 2.0-Ga-old metamorphosed oil-shale and generation of petroleum: geology, lithology and geochemistry. *Earth-Sci. Rev.* **47**, 1–40 (1999).
52. Paiste, K. *Reconstructing the Paleoproterozoic Sulfur Cycle: Insights from the Multiple Sulfur Isotope Record of the Zaonega Formation, Karelia, Russia*. PhD thesis, Univ. Tromsø (2018).
53. Siebert, C., Nägler, T. F. & Kramers, J. D. Determination of molybdenum isotope fractionation by double-spike multicollector inductively coupled plasma mass spectrometry. *Geochem. Geophys. Geosyst.* **2**, 1032 (2001).
54. Nägler, T. F. et al. Proposal for an international molybdenum isotope measurement standard and data representation. *Geostand. Geoanal. Res.* **38**, 149–151 (2014).
55. Mänd, K. et al. *Trace Metal Concentrations and Isotope Compositions from Drill Core OnZaP of the Zaonega Formation, NW-Russia* (PANGAEA, 2020); https://doi.org/10.1594/PANGAEA.911670
56. Mänd, K. et al. *Trace Metal Concentrations and Isotope Compositions from Drill Core OPH of the Zaonega Formation, NW-Russia* (PANGAEA, 2020); https://doi.org/10.1594/PANGAEA.911674

Acknowledgements

E. Ponzevera, A. De Prunelé, M. L. Rouget, C. Liorzou, K. von Gunten and F. Zhang are thanked for help with trace element and isotope analyses. K.M., K.K., A.L., T.K., P.P. and K.P. were supported by Estonian Research Council grant PRG447. K.M. was further supported by the Ministry of Education and Research of Estonia mobility grant within Archimedes Foundation's The Kristjan Jaak Scholarship program 'Doctoral Study Abroad'; K.P. was supported by the Research Council of Norway through its Centres of Excellence funding scheme grant no. 223259; A.E.R. acknowledges support from the state assignment of IG KarRC RAS; N.J.P. and C.T.R. acknowledge support from the NASA Alternative Earths Astrobiology Institute; K.O.K. was supported by a Natural Sciences and Engineering Research Council of Canada Discovery grant (RGPIN-165831).

Author contributions

A.L., K.K., K.O.K., S.V.L. and K.M. conceived the study. K.M., K.P., T.K., A.E.R., K.K. and A.L. conducted the field studies and organized the sample acquisition. K.P., T.K., A.E.R., K.K. and A.L. provided the geological and sedimentary background. K.P. provided additional TOC data. K.M., L.J.R., S.V.L., M.T., P.P., C.T.R., K.L., A.V. and K.O.K. measured and interpreted the trace metal abundance data. M.T., S.V.L. and K.M. analysed and interpreted the Mo isotope data. N.J.P., L.J.R. and K.M. analysed and interpreted the U isotope data. S.V.L., T.K., P.P. and K.K. analysed and interpreted the in situ trace metal abundance. K.M. wrote the manuscript with input from all the co-authors.

Competing interests

The authors declare no competing interests.

Additional information

Supplementary information is available for this paper at https://doi.org/10.1038/s41561-020-0558-5.

Correspondence and requests for materials should be addressed to K.M.

Peer review information Primary Handling Editor: Rebecca Neely.

Reprints and permissions information is available at www.nature.com/reprints.